

Tiny Object Detection with Single Point Supervision

Haoran Zhu^a, Chang Xu^a, Ruixiang Zhang^a, Fang Xu^b, Wen Yang^{a,*}, Haijian Zhang^a and Gui-Song Xia^b

^aSchool of Electronic Information, Wuhan University, Wuhan 430072, China

^bSchool of Computer Science, Wuhan University, Wuhan 430072, China

ARTICLE INFO

Keywords:

Object detection
Tiny object detection
Point supervision

ABSTRACT

Tiny objects, with their limited spatial resolution, often resemble point-like distributions. As a result, bounding box prediction using point-level supervision emerges as a natural and cost-effective alternative to traditional box-level supervision. However, the small scale and lack of distinctive features of tiny objects make point annotations prone to noise, posing significant hurdles for model robustness. To tackle these challenges, we propose Point Teacher—the first end-to-end point-supervised method for robust tiny object detection in aerial images. To handle label noise from scale ambiguity and location shifts in point annotations, Point Teacher employs the teacher-student architecture and decouples the learning into a two-phase denoising process. In this framework, the teacher network progressively denoises the pseudo boxes derived from noisy point annotations, guiding the student network’s learning. Specifically, in the first phase, random masking of image regions facilitates regression learning, enabling the teacher to transform noisy point annotations into coarse pseudo boxes. In the second phase, these coarse pseudo boxes are refined using dynamic multiple instance learning, which adaptively selects the most reliable instance from dynamically constructed proposal bags around the coarse pseudo boxes. Extensive experiments on three tiny object datasets (*i.e.*, AI-TOD-v2, SODA-A, and TinyPerson) validate the proposed method’s effectiveness and robustness against point location shifts. Notably, relying solely on point supervision, our Point Teacher already shows comparable performance with box-supervised learning methods. Codes and models will be made publicly available.

1. Introduction

Despite the remarkable progress made in tiny object detection recently (Akshatha et al., 2023; Zhao et al., 2024; Huang et al., 2024), the success of modern tiny object detectors largely depends on the availability of large-scale high-quality annotations such as TinyPerson (Yu et al., 2020), AI-TOD (Wang et al., 2021; Xu et al., 2022a), and SODA (Cheng et al., 2023). However, obtaining high-quality annotations is particularly challenging for tiny objects, their intrinsic characteristics—occupying few pixels (less than 16×16) and lacking discriminative features—significantly increase the cost and difficulty of box annotation. Moreover, the extremely limited pixel footprint of tiny objects leads to highly sparse shape and feature information, making them resemble point-like distributions. This naturally raises an intriguing question: *can we simplify box annotations as point annotations to supervise tiny object detection?*

This question, although previously explored for generic objects (Chen et al., 2022; He et al., 2024; Luo et al., 2024; Yu et al., 2024; Chen et al., 2024; May et al., 2024), remains a significant challenge for tiny object detection due to the unique issues of small scale and ambiguous boundary. Specifically, existing point-supervised object detection (PSOD)

*Corresponding author

✉ zhuhaoran@whu.edu.cn (H. Zhu); xuchangeis@whu.edu.cn (C. Xu); zhangruixiang@whu.edu.cn (R. Zhang); xufang@whu.edu.cn (F. Xu); yangwen@whu.edu.cn (W. Yang); haijian.zhang@whu.edu.cn (H. Zhang); guisong.xia@whu.edu.cn (G. Xia)

ORCID(s): 0009-0003-0153-1305 (H. Zhu); 0000-0002-3078-0496 (C. Xu); 0000-0003-0704-2484 (R. Zhang); 0000-0003-4260-7911 (F. Xu); 0000-0002-3263-8768 (W. Yang); 0000-0001-8314-6563 (H. Zhang); 0000-0001-7660-6090 (G. Xia)

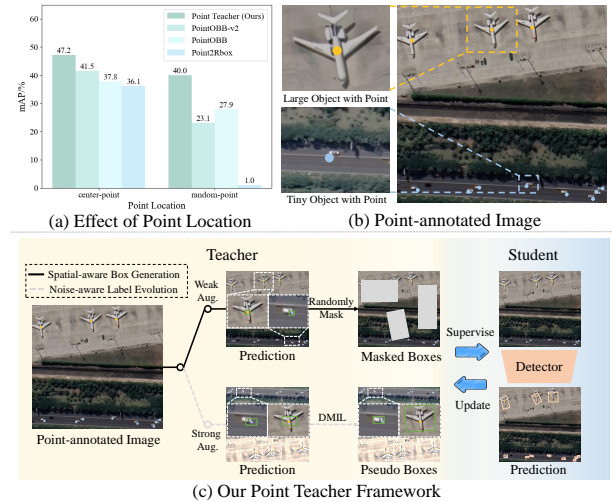


Figure 1: (a) Effect of point location on accuracy: previous methods assume that the point location lies within the center region, and performance significantly degrades when the point location slightly shifts around the center. (b) Comparison of point annotations for large and tiny objects: the limited scale and ambiguous boundaries make it challenging to annotate accurately on the main body of the tiny object. (c) An overview of our proposed Point Teacher: we propose a one-step two-phase learning paradigm that is robust to point location, consisting of Spatial-aware Box Generation and Noise-aware Label Evolution.

methods generally impose strong prior assumptions on the point location, such as center-point (Yu et al., 2024), center-region (Luo et al., 2024), gaussian-region (Chen et al., 2022), or mask-region (He et al., 2024) priors. These assumptions,

despite being beneficial for optimizing models in the generic scenarios, will not hold anymore for tiny objects, leading to a collapse in performance (Figure 1(a)). This collapse can be largely attributed to the noisy distribution of point annotations for tiny objects: the extremely limited scale and ambiguous boundaries not only make it challenging to ensure that point annotations accurately fall on the main body of the object but also render models particularly susceptible to location noise (Figure 1(b)).

To bridge the gap between the challenges posed by noisy point annotations and the need for accurate tiny object detection, we introduce **Point Teacher** (Figure 1(c))—a point-supervised method robust to location noise with a denoising-based training approach. In the previous point-to-box training, the lack of scale information and noisy point annotations significantly reduce the quality of generated pseudo boxes, severely undermining the effectiveness of the supervision signal for box prediction. Point Teacher tackles this challenge by converting the PSOD task for tiny objects into a two-phase box generation and denoising process: the first phase converts noisy point annotations to coarse box predictions, and the second phase progressively refines box quality by learning to denoise bounding boxes. We name each phase as **Spatial-aware Box Generation** and **Noise-aware Label Evolution**, respectively. Despite different phases, the entire model is trained in an end-to-end manner. Remarkably, unlike previous methods that rely on auxiliary knowledge (*e.g.*, synthesizing objects or using SAM-based models) for point-to-box generation, our approach eliminates the usage of auxiliary knowledge with a self-supervised learning strategy that enables the network to directly infer the coarse scale of tiny objects.

More specifically, in the Spatial-aware Box Generation phase, we randomly mask out parts of the image and enforce the network to predict the scale and location of the masked regions, granting the network an initial sense of spatial awareness (*i.e.*, box regression ability). In the subsequent Noise-aware Label Evolution phase, we introduce a Dynamic Multiple Instance Learning (DMIL) module to refine the noisy pseudo boxes generated by the teacher network, providing cleaner supervision for the student network. Compared to previous MIL modules, our DMIL dynamically extends object bags and corrects each proposal's locations within the bag. This location adjustment enhances the reliability of bag generation, even when point annotations are noisy. Additionally, we propose a simple yet effective noise-robust regression loss, termed Jittering IoU Loss, to mitigate overfitting to noisy pseudo boxes. Jittering IoU Loss applies controlled, small perturbations to the regression targets, encouraging the model to learn from multiple nearby target locations. This allows the model to better capture the overall target distribution, avoiding overfitting to specific noisy boxes.

Our Point Teacher can be seamlessly integrated into various detector architectures, supporting both horizontal bounding box (HBB) and oriented bounding box (OBB) tasks. Comprehensive experiments conducted on tiny object datasets (*i.e.*, AI-TOD-v2, TinyPerson, and SODA-A)

demonstrate the robustness and effectiveness of the proposed method. The main contributions of this paper are three-fold:

- We propose Point Teacher, the first end-to-end point-supervised framework for tiny object detection, specifically designed to address the challenge of achieving accurate detection under noisy point annotations.
- Our Point Teacher decouples the learning process into a two-phase denoising learning paradigm, comprising the Spatial-aware Box Generation phase and Noise-aware Label Evolution phase, to ensure robust performance under noisy point supervision.
- We demonstrate that our Point Teacher is highly generalizable to off-the-shelf object detectors and supports both horizontal bounding box (HBB) and oriented bounding box (OBB) tasks, achieving state-of-the-art results on point-based tiny object datasets under both center-based and noisy point annotation.

The rest of this paper is organized as follows. In Section 2, we briefly survey related works. In Section 3, we introduce the details of Point Teacher. Then, we validate the robustness and effectiveness of the proposed method in Section 4 and provide a detailed discussion in Section 5. Finally, we conclude this paper in Section 6.

2. Related Work

2.1. Tiny Object Detection

The extremely limited pixel count in tiny objects poses significant challenges for generic object detectors, leading to a surge in specialized research targeting this issue. In short, we can distinguish methods designed for tiny object detection as follows.

(a) **Multi-scale image and feature representations.** At the image level, techniques such as SNIP (Singh and Davis, 2018) and SNIPer (Singh et al., 2018) normalize object scales within a specific range to achieve scale-invariant detection. At the feature level, methods like Feature Pyramid Networks (FPN) have become foundational for multi-scale detection strategies (Lin et al., 2017a; Zheng et al., 2020; Deng et al., 2018), with advancements including PANet (Liu et al., 2018), Recursive-FPN (Tan et al., 2020), BiFPN (Qiao et al., 2021), TridentNet (Li et al., 2019), and Denoising-FPN (Liu et al., 2024a), which refine these approaches. Recent works by Wang et al. (Wang et al., 2024), Xiao et al. (Xiao et al., 2024), and Peng et al. (Peng et al., 2024) have introduced novel feature fusion strategies that enhance the representation of tiny objects by effectively integrating both global and local features. (b) **Super resolution.** In addition to multi-scale techniques, super-resolution-based detectors have emerged as a powerful approach for enhancing the feature representation by effectively reconstructing high-resolution features from limited pixel information (Bai et al., 2018; Li et al., 2017; Noh et al., 2019; Deng et al., 2018; Liu et al., 2024b). These methods leverage advancements in generative models and image enhancement to amplify subtle details,

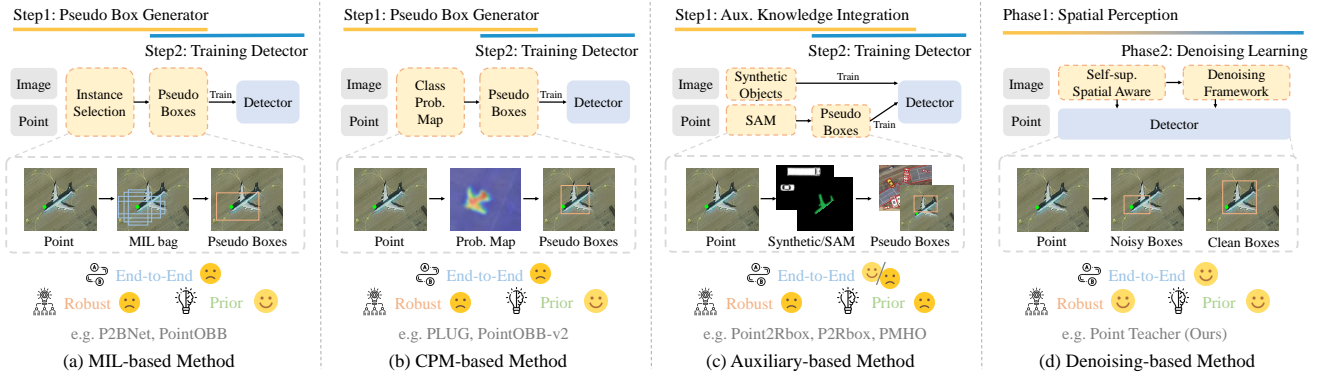


Figure 2: A comparison with existing point-supervised object detection methods, including (a) MIL-based methods; (b) CPM-based methods; (c) Auxiliary-based methods; (d) Denoising-based methods. (a), (b), and (c) paradigms adopt a two-step, non-end-to-end training process. (d) paradigm adopts a one-step, two-phase end-to-end training process. SAM denotes Segment Anything Model.

thereby improving detection accuracy for tiny objects. (c) **Learning strategies.** Recent advances have also shed new light on the learning strategies for tiny object detection (TOD). Notably, recognizing the vulnerability of Intersection over Union (IoU) to box offsets, several works have introduced new metrics for more accurate assignment (Xu et al., 2022a, 2021a; Tang et al., 2022; Shi et al., 2024). Furthermore, more recent approaches (Xu et al., 2022b, 2023) (e.g., RFLA) have developed scale-balanced assignment strategies to provide more effective supervision for tiny objects.

Previous works have made significant strides in tiny object detection under the assumption of a fully labeled training set. However, in real-world scenarios, obtaining fully annotated datasets is prohibitively costly. This work, instead, seeks to achieve robust and efficient learning under point supervision.

2.2. Point-supervised Object Detection

Training with point annotations has garnered considerable attention due to its low annotation cost. To achieve bounding box prediction with only point supervision, a widely adopted approach is the two-step point-to-box conversion. The first step involves training a model to generate pseudo boxes from point annotations, while the second step utilizes the generated pseudo boxes to train the object detector. Based on the way of generating pseudo boxes, existing methods can be categorized as follows (Figure 2).

(a) **MIL-based methods.** MIL-based methods typically begin by training a Multiple Instance Learning (MIL) model to generate pseudo boxes, which are then used to train the detector. Papadopoulos et al. (Papadopoulos et al., 2017) have proposed center-click annotation as a replacement for box annotation, using MIL to refine the localization process. UFO2 (Ren et al., 2020) introduces a unified weakly supervised detection framework, leveraging MIL to learn and localize targets from various types of annotations such as tags, points, scribbles, or boxes. Omni-DETR (Wang et al., 2022) extends UFO2 by supporting more forms of mixed annotations, leading to improved detection accuracy.

However, these MIL methods are based on OTSP approaches and are not specifically designed for point supervision tasks. P2BNet (Chen et al., 2022) first introduces an improved MIL framework tailored for point supervision, significantly improving the quality of pseudo-box generation. PointOBB (Luo et al., 2024) builds upon P2BNet by incorporating a self-supervised loss to learn angle and scale information, applying it to oriented object detection. Zhang et al. (Zhang et al., 2025) extend these methods to a sparse point annotation setting, substantially reducing the annotation cost. (b) **CPM-based methods.** CPM-based methods train a classification head to produce a Class Probability Map (CPM), which is subsequently used to generate pseudo boxes for training the detector. PLUG (He et al., 2024) refines the point-to-box process by introducing a point-mask-box framework, where the CPM is used to generate masks that facilitate the generation of pseudo boxes. PointOBB-v2 (Ren et al., 2024) enhances this process by proposing a non-uniform positive and negative sampling strategy for training the CPM, thereby achieving more accurate mask generation. (c) **Auxiliary-based methods.** Auxiliary-based methods consist of two subcategories distinguished by the source of auxiliary knowledge: synthetic-based and SAM-based methods. Synthetic-based methods manually synthesize objects or patterns as pseudo labels for end-to-end training, while SAM-based methods refine the detection process using masks generated by the Segment Anything Model (SAM) (Kirillov et al., 2023). Point2Rbox (Yu et al., 2024), as a synthetic-based method, introduces synthetic knowledge and constructing synthetic objects to learn regression capabilities, enabling end-to-end oriented object detection. P2RBox (Cao et al., 2023) and PMHO (Zhang et al., 2024) adopt the point-mask-box paradigm and integrate the SAM (Kirillov et al., 2023) model, resulting in a significant performance boost for the network.

While these methods have advanced point-supervised object detection, they primarily assume that point locations are centered or within central regions. This assumption is too rigorous for tiny objects with minimal pixel occupancy,

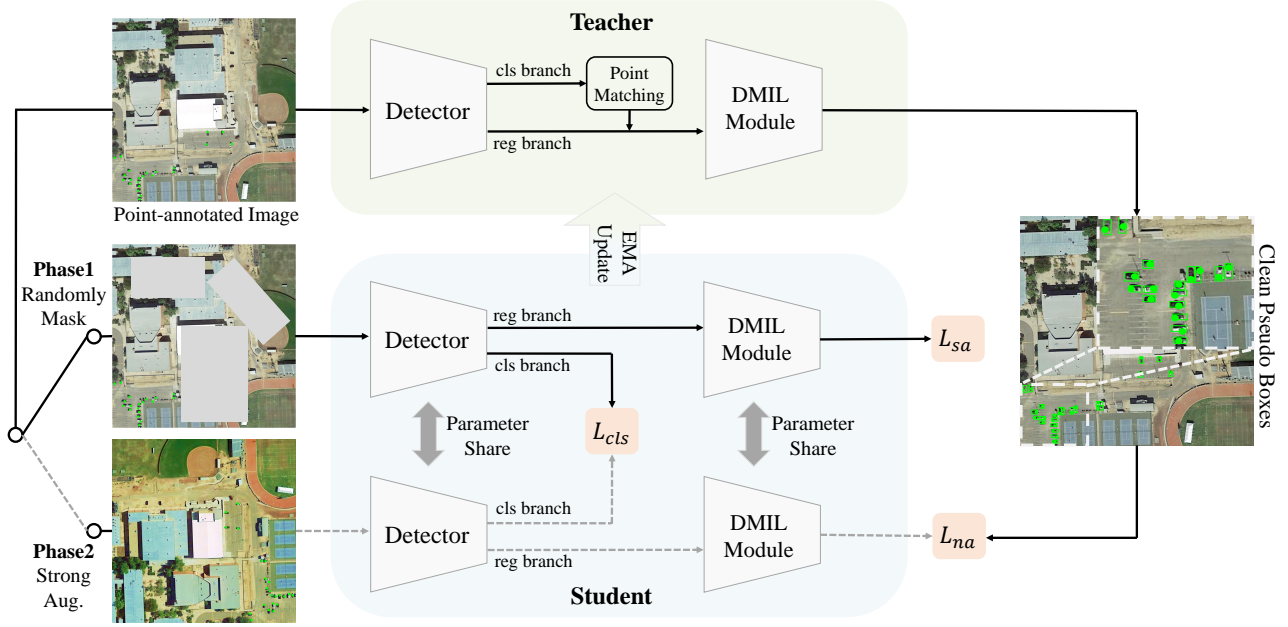


Figure 3: The framework of Point Teacher. The training process of Point Teacher consists of two phases: Spatial-aware Box Generation (phase1) and Noise-aware Label Evolution (phase2). During the Spatial-aware Box Generation phase, the masked image is used to train both the regression branch and the DMIL module, enabling the model to develop spatial awareness. In the Noise-aware Label Evolution phase, the teacher network, in conjunction with the DMIL module, generates clean pseudo boxes to supervise the student network for end-to-end learning. The classification learning is integrated throughout the phases.

as even slight positional shifts can lead to a significant drop in accuracy due to the sensitivity of tiny objects to location. Additionally, the aforementioned methods adopt a two-step, non-end-to-end paradigm, which typically requires more time to implement the point-to-box detection training process. Thus, in this paper, we focus on the impact of point location on network performance and propose Point Teacher, a robust, end-to-end denoising-based PSOD method.

3. Methodology

3.1. Overall Framework

This work proposes an end-to-end point-supervised tiny object detector. Unlike previous two-step methods (Chen et al., 2022; Yu et al., 2024; Luo et al., 2024; Ren et al., 2024), which first train a pseudo-box generator and then a detector, we introduce an end-to-end denoising-based method consisting of the Spatial-aware Box Generation phase and Noise-aware Label Evolution phase, as shown in Figure 3. Both phases are integrated into a unified pipeline, enabling direct optimization from point annotations to the final detection output. In the Spatial-aware Box Generation phase, the network is trained to develop spatial awareness and learn the mapping from points to coarse pseudo boxes. In the subsequent Noise-aware Label Evolution phase, the network undergoes denoising learning to refine the coarse pseudo boxes into precise pseudo boxes. Additionally, as the annotated point provides both class information and rough positional cues, object classification is performed

throughout the entire process. The overall loss function can be summarized as:

$$L = L_{cls} + L_{sa} + L_{na}, \quad (1)$$

where L_{cls} represents the classification loss from the detection head. L_{sa} and L_{na} denote the loss during the Spatial-aware Box Generation phase and Noise-aware Label Evolution phase, respectively. During inference, only the detector is utilized.

Additionally, since Point Teacher is orientation-agnostic, it is applicable to both Horizontal Bounding Box (HBB) and Oriented Bounding Box (OBB) detection tasks. In the final part of this section, we will demonstrate how to deploy the method on HBB detectors. For OBB detectors, the only required adjustment is the incorporation of the angle parameter θ .

3.2. Spatial-aware Box Generation

The point-based annotation lacks both scale and precise location information of objects, making it impractical to regress bounding box solely from point supervision. Inspired by DINOv2's self-supervised approach for learning robust visual features, which masks random image patches to ensure feature consistency (Oquab et al., 2023), we adapt this strategy for the box regression task to help the network develop spatial awareness. Specifically, we randomly mask certain regions of the image: $R(\{cx, cy, w, h\})$ for HBB task and $\{cx, cy, w, h, \theta\}$ for OBB task). The regression head is then tasked with predicting the scale and position of the

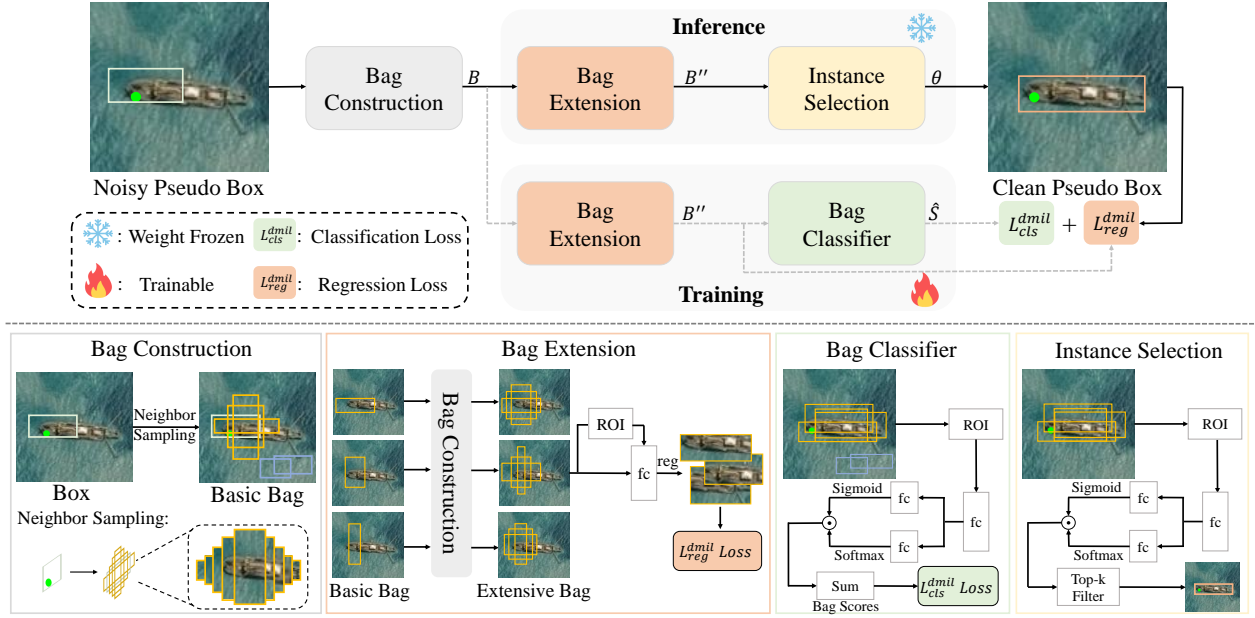


Figure 4: The workflow of Dynamic Multiple Instance Learning Module (DMIL). DMIL comprises four stages: Bag Construction, Bag Extension, Bag Classifier, and Instance Selection. The Bag Construction and Bag Extension stages ensure the creation of high-quality bags. The Bag Classifier is used to train the classification and discrimination capabilities of the bags. Finally, Instance Selection uses the scores from the Bag Classifier to merge instances, generating pseudo boxes.

masked region. The supervision for this task is provided by the loss term L_{reg}^{sa} , which is computed for each masked region R .

$$L_{reg}^{sa} = L_{bbox}(P, R), \quad (2)$$

where P denotes the network's prediction, with P representing $\{cx, cy, w, h\}$ for the HBB task and $\{cx, cy, w, h, \theta\}$ for the OBB task. The term L_{bbox} represents the regression loss, such as Smooth L1 Loss or IoU-based Loss. In this work, we use the Jittering IoU Loss, which will be described in detail in the following section 3.3.

Mask region regression enhances the model's spatial awareness by leveraging a regression-driven guidance mechanism. However, MIL-based methods construct bags by applying fixed-scale jittering around coarse pseudo boxes, which lacks the flexibility to dynamically adjust bag construction based on spatial awareness (Wu et al., 2023). To address this limitation, we introduce a Dynamic Multiple Instance Learning (DMIL) module. As illustrated in Figure 4, DMIL comprises four key processes: **Bag Construction**, **Bag Extension**, **Bag Classifier**, and **Instance Selection**. Our DMIL emphasizes extending the constructed bags and introducing a regression branch to refine proposals, enabling improved spatial awareness and more accurate pseudo-box generation. For clarity, we illustrate the DMIL framework using the HBB task as an example. When extending to the OBB task, it suffices to incorporate the angle parameter θ into all bounding boxes and replace the RoI extractor (Ren et al., 2017) with a Rotated RoI extractor (Ding et al., 2019).

Given an image containing M coarse pseudo boxes $Z \in \mathbb{R}^{M \times 4}$ (generated by the teacher network) and N masked

regions $R \in \mathbb{R}^{N \times 4}$. we first perform **Bag Construction** for each box in Z and R . This process generates pseudo-box proposal bags $B_Z \in \mathbb{R}^{M \times U_1 \times 4}$, mask proposal bags $B_R \in \mathbb{R}^{N \times U_1 \times 4}$, and negative proposals $B_{neg} \in \mathbb{R}^{U_{neg} \times 4}$, where U_1 and U_{neg} represent the number of proposals in each bag and the number of negative proposals in an image. The bag construction process follows the neighbor sampling strategy used in P2BNet (Chen et al., 2022).

Since all the bags are sampled near the coarse pseudo boxes, they may be inaccurate. Therefore, in **Bag Extension** stage, we extend and refine the bags to ensure that more precise proposals can be sampled. For each proposal in bag B_Z and B_R , we perform neighbor sampling to expand it into an augmented set, $B'_Z \in \mathbb{R}^{M \times U_1 \times U_2 \times 4}$ and $B'_R \in \mathbb{R}^{N \times U_1 \times U_2 \times 4}$, where U_2 denotes the number of newly generated proposals during the bag extension process. Then, we refine the proposals in B'_Z and B'_R to obtain more accurate proposal bags. Specifically, using 7×7 RoIAlign and two fully connected (fc) layers, the features of the proposals in B'_Z and B'_R are extracted, denoted as $F'_Z \in \mathbb{R}^{M \times U_1 \times U_2 \times D}$ and $F'_R \in \mathbb{R}^{N \times U_1 \times U_2 \times D}$. The regressor then takes the proposal bag and features as input and outputs a refined bag $B''_Z \in \mathbb{R}^{M \times U_1 \times U_2 \times 4}$ and $B''_R \in \mathbb{R}^{N \times U_1 \times U_2 \times 4}$. Note that at this phase (*i.e.*, Spatial-aware Box Generation phase), we possess the reliable localization information of masked regions R . Thus, we can leverage them to supervise the training of the regressor. Since the supervision signals within the same bag are consistent, we replicate R by $U_1 \times U_2$ times to obtain $R' \in \mathbb{R}^{N \times U_1 \times U_2 \times 4}$. The corresponding loss is denoted as:

$$L_{reg}^{dmil} = L_{bbox}(B''_R, R'). \quad (3)$$

After constructing and extending the bags, it is essential to equip DMIL with the ability to select high-quality proposals from each bag. Thus, in the **Bag Classifier** stage, we focus on training DMIL's classifier and instance selector. It is worth noting that since the R lacks class information, we do not apply the Bag Classifier and Instance Selection operations to B_R'' . Consequently, we pass B_Z'' through RoIAlign and two fully connected (fc) layers (without sharing weights with the regressor's fc) to generate features $F_Z'' \in \mathbb{R}^{M \times U_1 \times U_2 \times D}$. We then apply the classification branch f_{cls} to F_Z'' , yielding $O^{cls} \in \mathbb{R}^{M \times U_1 \times U_2 \times C}$, which is then passed through the *sigmoid* function over the classification dimension to obtain the score S^{cls} , where C represents the number of category. Meanwhile, we apply the instance branch f_{ins} to F_Z'' , yielding $O^{ins} \in \mathbb{R}^{M \times U_1 \times U_2 \times C}$, and S^{ins} is obtained through *softmax* function over U_2 proposals. During training, the score S for each proposal is computed as the Hadamard product of S^{cls} and S^{ins} . Subsequently, the scores of all proposals within the bag are summed to obtain the final score for each bag, $\hat{S} \in \mathbb{R}^{M \times U_1 \times C}$.

$$\begin{cases} O^{cls} = f_{cls}(F_Z''); & S_{i,j,k,c}^{cls} = 1/(1 + e^{-O_{i,j,k,c}^{cls}}) \\ O^{ins} = f_{ins}(F_Z''); & S_{i,j,k,c}^{ins} = e^{O_{i,j,k,c}^{ins}} / \sum_{x=1}^{U_2} e^{O_{i,j,x,c}^{ins}} \\ S = S^{cls} \odot S^{ins}; & \hat{S}_{i,j,c} = \sum_{k=1}^{U_2} S_{i,j,k,c} \end{cases} \quad (4)$$

where $S_{i,j,k,c}$ represents the element value at the (i, j, k, c) index. The *sigmoid* activation is applied to each position (i, j, k, c) of S^{cls} along the class dimension C , while the *softmax* activation is applied to each position (i, j, k, c) of S^{ins} along the proposal dimension U_2 .

The supervision for training DMIL's classifier and instance selector is provided by the loss term L_{cls}^{dmil} , which is computed for each bag B_Z'' and the negative proposals B_{neg} . Note that negative proposals do not form bags. Thus, they only have classification scores $\hat{S}^{neg} \in \mathbb{R}^{U_{neg} \times C}$ without instance scores. The loss L_{cls}^{dmil} is defined as follows:

$$L_{cls}^{dmil} = L_{cls}(\hat{S}, \xi^{pos}) + L_{cls}(\hat{S}^{neg}, \xi^{neg}), \quad (5)$$

where $\xi^{pos} \in \{0, 1\}^{M \times U_1 \times C}$, $\xi^{neg} \in \{0\}^{U_{neg} \times C}$. The term L_{cls} represents the classification loss. In this work, we use the Focal Loss (Lin et al., 2017c).

During the **Instance Selection** stage, classification and instance scores are utilized to select the top- k scoring proposals from each bag as pseudo boxes. Specifically, we first reshape S and B_Z'' into $\mathbb{R}^{M \times (U_1 \cdot U_2) \times C}$ and $\mathbb{R}^{M \times (U_1 \cdot U_2) \times 4}$. Then, for each coarse pseudo box Z_j , we filter the extension bag to select the top- k most accurate proposals, merging them with the coarse pseudo boxes Z_j to generate precise pseudo boxes Θ_j .

$$\Theta_j = \beta \cdot Z_j + (1 - \beta) \cdot \sum_{i=1}^k S_{jic} \cdot B_{ji}'', \quad \text{where } \sum_{i=1}^k S_{jic} = 1, \quad (6)$$

β represents the weighted fusion coefficient, a hyperparameter between 0 and 1.

In summary, the loss for the Spatial-aware Box Generation phase can be formulated as follows:

$$L_{sa} = L_{reg}^{sa} + \alpha_1 \cdot L_{reg}^{dmil} + \alpha_2 \cdot L_{cls}^{dmil}, \quad (7)$$

where α_1 and α_2 are set as 0.01 and 0.25 respectively.

3.3. Noise-aware Label Evolution

After the Spatial-aware Box Generation phase, the network achieves coarse spatial awareness, allowing the teacher network to predict coarse pseudo boxes. In the Noise-aware Label Evolution phase, we further refine the coarse pseudo boxes and perform denoising training.

Following the typical teacher-student architecture (Xu et al., 2021b), we use the pseudo boxes generated by the teacher network to supervise the student network for high-quality training. However, our approach differs from previous methods in two key aspects: (1) **Point Matching**: Unlike previous methods like Soft Teacher (Xu et al., 2021b), which determine pseudo boxes solely based on a classification score threshold (≥ 0.9), our approach additionally leverages the positional information from point annotations to better guide pseudo box generation. (2) **Box Refinement**: The pseudo boxes produced by the teacher network in the PSOD task are more coarse and unsuitable for direct supervision of the student network. Thus, we leverage DMIL and Jittering IoU Loss to refine these pseudo boxes, enabling more precise box generation and robust learning for the regression branch. Note that, in the previous Spatial-aware Box Generation phase, we solely train DMIL to enhance spatial awareness without refining pseudo boxes. In this phase, however, we will further apply DMIL to refine the pseudo boxes.

Point Matching: Instead of using classification scores alone to determine pseudo boxes, our approach benefits from the guidance provided by the rough positional information of point annotations. To achieve the best matching between the annotated points and the predicted boxes, we propose a two-stage Top- K point matching method. Specifically, we first filter the Top- K_1 candidate boxes based on their L_1 distance to the annotated points. Next, from these K_1 candidates, we select the Top- K_2 boxes using a cost matrix, which helps merge and generate pseudo boxes. The cost matrix consists of two main components: classification cost and spatial cost:

$$\text{Cost}(i, j) = \underbrace{(L_{cls}(s_{ji}, c_j))}_{\text{classification cost}} + \underbrace{(1 - \mathbb{1}[p_j \text{ in } b_{ji}])}_{\text{spatial cost}}, \quad (8)$$

where j is the index of the annotated point, and i is the index of the predicted box. p_j and c_j represent the annotated point and its category. s_{ji} and b_{ji} denote the classification scores and prediction boxes belonging to annotated point p_j . The term $(1 - \mathbb{1}[p_j \text{ in } b_{ji}])$ indicates that the cost is 0 when the annotated point lies within the predicted box; otherwise, the cost is 1.

Finally, we perform a box fusion based on the classification scores s to generate the coarse pseudo boxes Θ_j . The

fusion formula is as follows:

$$\Theta_j = \sum_{k=1}^{K_2} s_{jk} \cdot b_{jk}, \quad \text{where } \sum_{k=1}^{K_2} s_{jk} = 1. \quad (9)$$

Box Refinement: After obtaining the coarse pseudo boxes, the randomness of the annotated point leads to pseudo boxes with potential offsets and scale variations. To provide the student network with high-quality pseudo boxes, we first perform Bag Construction and Bag Extension for Θ_j , generating the candidate proposals Bag B_j'' and proposal scores S_j . These are then passed to the Bag Classifier and Instance Selection stages, where the Top- K_3 most accurate proposals are chosen to generate the refined pseudo boxes Θ_j' . The fusion method is as follows:

$$\Theta_j' = \beta \cdot \Theta_j + (1-\beta) \cdot \sum_{k=1}^{K_3} S_{jk} \cdot B_{jk}'', \quad \text{where } \sum_{k=1}^{K_3} S_{jk} = 1. \quad (10)$$

During training, we use the generated pseudo boxes Θ' to supervise both the regression branch of the detection head and the regression branch of DMIL. Additionally, the classifier in DMIL remains unchanged. The overall loss function is:

$$\begin{cases} L_{reg}^{na} = L_{bbox}(P, \Theta') \\ L_{reg}^{dmil} = L_{bbox}(B'', \Theta') \\ L_{na} = L_{reg}^{na} + \alpha_1 \cdot L_{reg}^{dmil} + \alpha_2 \cdot L_{cls}^{dmil}. \end{cases} \quad (11)$$

To further enhance the network's robustness and resistance to noisy pseudo boxes, we propose **Jittering IoU Loss**, a simple yet effective auxiliary regression loss. The loss encourages the model to learn across different, yet nearby target positions, enabling it to better capture the overall object distribution and avoid overfitting to specific noisy pseudo boxes (Li, 2024). Specifically, for HBB task, given a predicted box $A = (cx, cy, w, h)$ and a regression target $B_{gt} = (cx_{gt}, cy_{gt}, w_{gt}, h_{gt})$, we first expand and shrink B_{gt} by a certain ratio r to create perturbed versions B'_{gt} :

$$B'_{gt} = \begin{cases} (cx_{gt}, cy_{gt}, w_{gt}, h_{gt}) \\ (cx_{gt}, cy_{gt}, w_{gt} - w_{gt} \cdot r, h_{gt} - h_{gt} \cdot r) \\ (cx_{gt}, cy_{gt}, w_{gt} - w_{gt} \cdot r, h_{gt} + h_{gt} \cdot r) \\ \dots \\ (cx_{gt}, cy_{gt}, w_{gt} + w_{gt} \cdot r, h_{gt} + h_{gt} \cdot r). \end{cases} \quad (12)$$

For the OBB task, we keep the angle parameter unchanged and only perturb the parameters (cx, cy, w, h) . The final regression loss is composed of the base loss combined with the minimum loss derived from the perturbed targets.

$$L_{bbox} = L_{IoU}(A, B_{gt}) + \min_i L_{IoU}(A, B'_{gt}[i]). \quad (13)$$

3.4. Detector Integration

Our method is general and is not limited to specific object detectors. However, due to the lack of scale information in

point annotations, scale-aware components like FPN (Lin et al., 2017b) and Label Assignment in existing detectors such as FCOS (Tian et al., 2019) and Faster R-CNN (Ren et al., 2017) cannot be directly used. To address this issue, we replace the FPN and Label Assignment with the proposed **Top-down FPN Aggregation** and **Scale-invariant Label Assignment** in our method.

Top-down FPN Aggregation: Each layer of the FPN has feature points with varying receptive fields (Gong et al., 2021), typically used for detecting objects of different sizes, from small to large, across layers P_3 to P_7 . For tiny objects, the features are mainly allocated to the P_3 layer. To avoid scale confusion while still incorporating high-level semantic information, we propose a simple and effective Top-down FPN Aggregation strategy. Specifically, we use 1×1 convolution (*Conv*) and Upsampling (*Up*) operations to aggregate features from layers P_3 to P_7 into a single output layer M , as shown below:

$$\begin{cases} P_{i-1} = P_{i-1} + Up(Conv(P_i)), & i \in \{5, \dots, 7\} \\ M = P_{i-1} + Up(Conv(P_i)), & i = 4. \end{cases} \quad (14)$$

Scale-invariant Label Assignment: Existing label assignment algorithms heavily rely on accurate *gt* scale information. For instance, FCOS assigns positive samples within the center region of *gt* boxes, while Faster R-CNN designates positive samples when the IoU between anchors and *gt* boxes exceeds 0.5. However, in the absence of *gt* boxes, these assignment strategies cannot be applied. Therefore, we propose a one-to-one scale-invariant label assignment strategy. Specifically, we utilize the central points of the pseudo boxes generated by DMIL and select the nearest feature point as a positive sample based on the L1 distance to these central points.

4. Experiments

4.1. Experimental Settings

Point-annotated Dataset. We conduct comprehensive evaluations of our method on the AI-TOD-v2.0 (Xu et al., 2022a) dataset, a benchmark known for its challenging tiny object detection scenarios with an average object size of 12.7 pixels. Additionally, we validate the effectiveness of our method in small aerial object detection scenarios using the TinyPerson (Yu et al., 2020) and SODA (Cheng et al., 2023) datasets. Based on these datasets, we propose a method for generating point annotations. The location of the point is defined within a range m around the region of the *gt*, where m varies from 0% to 100%. Specifically, let $\{cx, cy, w, h\}$ and $\{cx, cy, w, h, \theta\}$ represent an object in the HBB and OBB tasks, respectively. We simulate an annotated point $\{px, py\}$ as follows:

$$\begin{cases} px_h = cx + \Delta_x \cdot w \\ py_h = cy + \Delta_y \cdot h \\ px_o = cx + \Delta_x \cdot w \cdot \cos\theta \\ py_o = cy + \Delta_y \cdot h \cdot \sin\theta, \end{cases} \quad (15)$$

Table 1

Comparison between the Point Teacher and other methods on the AI-TOD-v2.0 val set (HBB) and SODA-A (Cheng et al., 2023) val set (OBB) with **central annotated points** ($m = 0\%$). We report $AP_{0.25}$ in this table. Y denotes the end-to-end paradigm. We utilize FCOS as the detector except Point2Rbox-RC (YOLOF). * mean two-stage MIL.

Method	Type	E2E	VE	SH	PE/HE	ST	SP	AI	BR/CT	WM	mAP
<i>HBox-supervised detectors (AI-TOD-v2)</i>											
RetinaNet (Lin et al., 2017c)	HBB	Y	62.0	72.3	26.2	34.8	8.7	2.4	43.6	3.4	31.7
Faster R-CNN (Ren et al., 2017)	HBB	Y	49.0	56.2	19.7	40.6	60.2	38.6	30.9	5.7	37.6
FCOS (Tian et al., 2019)	HBB	Y	75.7	76.2	26.5	65.9	46.2	1.9	36.5	0.3	41.2
<i>Point-supervised detectors (AI-TOD-v2)</i>											
P2BNet (Chen et al., 2022)	HBB	N	0.9	1.9	0.0	7.6	0.1	0.0	1.2	0.0	1.5
P2BNet* (Chen et al., 2022)	HBB	N	0.1	0.8	1.1	16.7	0.0	0.1	0.3	0.0	2.4
PLUG (He et al., 2024)	HBB	N	19.4	51.5	10.0	14.9	54.0	1.2	1.9	0.7	19.2
Point Teacher	HBB	Y	58.2	62.8	17.5	47.1	43.2	1.3	45.4	8.7	35.5
<i>RBox-supervised detectors (SODA-A)</i>											
RetinaNet-O (Lin et al., 2017c)	OBB	Y	50.1	82.2	53.0	77.2	88.4	89.0	58.8	87.0	70.7
FCOS-O (Tian et al., 2019)	OBB	Y	61.9	87.4	51.5	81.6	88.6	89.8	60.2	88.7	74.6
Oriented R-CNN (Xie et al., 2021)	OBB	Y	61.0	87.1	56.0	84.9	88.6	89.6	55.5	88.9	74.7
<i>Point-supervised detectors (SODA-A)</i>											
PointOBB* (Luo et al., 2024)	OBB	N	11.7	13.7	56.0	19.7	45.3	80.4	22.8	78.7	37.8
Point2Rbox-RC (Yu et al., 2024)	OBB	Y	6.3	14.4	71.1	48.4	88.8	10.1	3.3	76.0	36.1
PointOBB-v2 (Ren et al., 2024)	OBB	N	26.3	66.4	50.5	55.0	41.4	56.0	44.6	7.2	41.5
Point Teacher	OBB	Y	43.9	77.6	27.5	22.5	85.8	31.8	19.0	72.9	47.2

where Δ_x and Δ_y follow the uniform distribution $U(-m/2, m/2)$. When $m = 0\%$, the point is placed at the center of the gt , while $m = 100\%$ allows the point to be located anywhere within the gt . Notably, to validate the robustness of Point Teacher, we conduct main experiments on AI-TOD-v2.0 and SODA-A under varying conditions with $m = 0\%$ to 100% . Ablation studies are performed specifically with $m = 0\%$ to ablate the effects of each component.

Implementation Details. Our implementation is based on the MMDetection (Chen et al., 2019) and MMRotate (Zhou et al., 2022) toolkits, built on the PyTorch (Paszke et al., 2019) deep learning framework. We employ an ImageNet (Russakovsky et al., 2015) pre-trained model as the backbone. Training is conducted for 12 epochs using the Stochastic Gradient Descent (SGD) optimizer, with a momentum of 0.9, a weight decay of 0.0001, and a batch size of 2. The initial learning rate is set to 0.005 and decreases at epochs 8 and 11. The Region Proposal Network (RPN) generates up to 3000 proposals. During inference, we filter background boxes with a confidence threshold of 0.05 and apply Non-Maximum Suppression (NMS) with an IoU threshold of 0.5, selecting the top 3000 bounding boxes. All other parameters remain consistent with the defaults in MMDetection and MMRotate. Given that IoU-based metrics are particularly unfavorable for tiny object detection (Xu et al., 2022a), $AP_{0.5}$ is not an ideal evaluation standard under point annotation scenarios. Therefore, we adopt $AP_{0.25}$ as an alternative evaluation metric in this work. The teacher model is an exponential moving average (EMA) of the student

model, with the EMA momentum set to the default value of 0.999 (Xu et al., 2021b). The fusion weight β for generating pseudo boxes is set to 0.25, while the shaking ratio r for Jittering IoU Loss is chosen to be 0.2. During fusion, K_1 , K_2 , and K_3 are set to 5, 3, and 1, respectively. The Spatial-aware Box Generation phase occurs during the first 4000 iterations of training, with the remaining iterations dedicated to the Noise-aware Label Evolution phase.

4.2. Main Results

We compare our method with state-of-the-art (SOTA) methods on the AI-TOD-v2.0 (Xu et al., 2022a) (horizontal object detection) and SODA-A (Cheng et al., 2023) (oriented object detection) datasets. As shown in Table 1, our method consistently outperforms all current SOTA algorithms on tiny object detection tasks. For the horizontal object detection task, we compare our approach with P2BNet (Chen et al., 2022) and PLUG (He et al., 2024), where P2BNet exhibits a weak performance of 2.4%. This is mainly because P2BNet, a MIL-based pseudo-boxes generator, relies solely on classification scores to filter pseudo boxes, but the weak features of tiny objects make the classification scores inaccurate in reflecting the quality of pseudo boxes. PLUG, a CPM-based pseudo-boxes generator, produces relatively accurate pseudo-boxes. However, due to the indistinct boundaries and color features of tiny objects, the segmentation loss in PLUG fails to converge effectively. In contrast, our method, after obtaining coarse pseudo boxes during the Spatial-aware Box Generation phase, leverages the spatially-aware DMIL

Table 2

Comparison between other methods and our proposed Point Teacher on the AI-TOD-v2.0 val set (HBB) and SODA-A (Cheng et al., 2023) val set (OBB) with **randomly annotated points** ($m = 100\%$).

Method	Type	E2E	VE	SH	PE/HE	ST	SP	AI	BR/CT	WM	mAP
<i>HBox-supervised detectors (AI-TOD-v2)</i>											
RetinaNet (Lin et al., 2017c)	HBB	Y	62.0	72.3	26.2	34.8	8.7	2.4	43.6	3.4	31.7
Faster R-CNN (Ren et al., 2017)	HBB	Y	49.0	56.2	19.7	40.6	60.2	38.6	30.9	5.7	37.6
FCOS (Tian et al., 2019)	HBB	Y	75.7	76.2	26.5	65.9	46.2	1.9	36.5	0.3	41.2
<i>Point-supervised detectors (AI-TOD-v2)</i>											
P2BNet (Chen et al., 2022)	HBB	N	0.2	0.5	0.0	1.8	0.0	0.0	0.5	0.0	0.4
P2BNet* (Chen et al., 2022)	HBB	N	0.6	0.7	0.8	5.5	0.0	0.1	3.4	0.0	1.4
PLUG (He et al., 2024)	HBB	N	3.8	2.3	2.0	4.1	48.3	3.0	3.0	0.0	8.3
Point Teacher	HBB	Y	54.5	63.1	16.2	40.4	33.9	0.7	41.9	2.3	31.6
<i>RBox-supervised detectors (SODA-A)</i>											
RetinaNet-O (Lin et al., 2017c)	OBB	Y	50.1	82.2	53.0	77.2	88.4	89.0	58.8	87.0	70.7
FCOS-O (Tian et al., 2019)	OBB	Y	61.9	87.4	51.5	81.6	88.6	89.8	60.2	88.7	74.6
Oriented R-CNN (Xie et al., 2021)	OBB	Y	61.0	87.1	56.0	84.9	88.6	89.6	55.5	88.9	74.7
<i>Point-supervised detectors (SODA-A)</i>											
PointOBB* (Luo et al., 2024)	OBB	N	3.3	2.2	49.4	5.4	65.8	48.6	0.5	72.6	27.9
Point2Rbox-RC (Yu et al., 2024)	OBB	Y	0.0	0.5	0.1	0.1	7.3	0.0	0.0	1.3	1.0
PointOBB-v2 (Ren et al., 2024)	OBB	N	10.1	42.8	22.5	43.9	12.4	56.0	8.0	2.2	23.1
Point Teacher	OBB	Y	16.6	34.2	42.2	62.7	43.8	71.3	13.0	59.3	40.0

Table 3

Robustness of other methods and our proposed Point Teacher performance with the point location m set to 0%, 30%, 60%, and 100%. * means two-stage MIL.

m	Point Teacher	PLUG	P2BNet*	P2BNet
0%	35.5	19.2	2.4	1.5
30%	36.3	16.7	5.7	1.0
60%	33.0	13.5	3.4	0.6
100%	31.6	8.3	1.4	0.4

module to generate more stable and accurate pseudo boxes, thereby improving detection performance by 16.3%. For the oriented object detection task, we compare our approach with PointOBB (Luo et al., 2024), PointOBB-v2 (Ren et al., 2024) and Point2Rbox (Yu et al., 2024). Although PointOBB remains a MIL-based method, the issue of classification scores is mitigated due to the relatively larger object sizes in the SODA-A dataset, resulting in a significant improvement in accuracy of 37.8%. Point2Rbox, as an Auxiliary-based method, also demonstrates strong competitiveness. However, it is important to note that the indistinct features of tiny objects create a domain gap between the synthetic objects and the real tiny objects, limiting their generalization ability. During training, the network tends to overfit the features of the synthetic objects, which deteriorates the regression branch. In contrast, our method alleviates this issue by utilizing pseudo boxes generated by DMIL for supervision, leading to an

Table 4

Comparison between other methods and our proposed Point Teacher on the TinyPerson (Yu et al., 2020) test set with central annotated points. We report $AP_{0.25}$ in this table. We utilize FCOS as the detector.

Method	mAP	AP_{ct}	AP_t	AP_s	AP_m
<i>Hbox-supervised detectors</i>					
RetinaNet	13.9	2.3	7.0	16.1	33.9
Faster R-CNN	15.6	0.0	3.8	19.2	52.2
FCOS	34.2	9.1	24.2	43.5	68.8
<i>Point-supervised detectors</i>					
P2BNet	2.3	0.0	1.0	4.0	8.3
P2BNet*	7.9	0.0	2.4	14.1	24.2
PLUG	7.4	0.0	1.0	8.9	28.1
Ours	18.6	3.8	19.3	24.4	29.4

improvement in performance by 11.1%. Unlike the significant improvement observed in the HBB task, the performance of the Point Teacher on the OBB task is relatively lower. This is primarily because our method is directly transferred from HBB to OBB without any refinement or dedicated design to address angle-related issues.

We also conduct experiments on the TinyPerson (Yu et al., 2020) dataset. The results, as shown in Table 4, demonstrate that our method achieves competitive performance, reaching 54.4% of hbox-supervised accuracy.

Table 5

Ablations. We train on point-based AI-TOD-v2.0 train set, test on val set. Phase1 and Phase2 represent Spatial-aware Box Generation phase and Noise-aware Label Evolution phase respectively. Gray row means default setting.

(a) Individual effectiveness of components in Point Teacher.

Phase1	Phase2			mAP
Randomly Mask	Teacher-Student	DMIL	Jittering IoU Loss	
✓				21.0
✓	✓			24.5
✓	✓	✓		34.7
✓	✓	✓	✓	35.5

(b) Comparison of DMIL and MIL. * denotes two-stage MIL.

Method	mAP	AP _{vt}	AP _t	AP _s	AP _m
MIL	20.0	10.0	27.6	18.3	17.4
MIL*	20.3	9.7	29.6	15.7	22.9
DMIL	35.5	17.5	42.0	37.4	26.6

(c) $\{K_1, K_2, K_3\}$ for Pseudo Boxes Generation.

K_1	K_2	K_3	mAP	AP _{vt}	AP _t	AP _s	AP _m
3	1	1	28.2	25.3	31.8	42.7	0.4
3	1	5	33.6	28.2	37.1	44.3	14.4
5	3	1	35.5	17.5	42.0	37.4	26.6
5	3	5	31.9	10.3	47.3	30.1	55.5

(d) r in Jittering IoU Loss.

r	mAP	AP _{vt}	AP _t	AP _s	AP _m
0.0	34.7	12.4	44.5	32.0	21.9
0.2	35.5	17.5	42.0	37.4	26.6
0.4	33.2	6.3	56.0	30.2	57.0
0.6	33.0	5.6	44.1	37.6	49.1

(e) β in DMIL Fusion.

β	mAP	AP _{vt}	AP _t	AP _s	AP _m
0.00	34.7	22.6	40.9	46.6	10.9
0.25	35.5	17.5	42.0	37.4	26.6
0.50	31.6	13.9	44.0	29.9	58.8
1.00	24.5	5.4	38.8	23.1	32.1

(f) Training proportion of the Spatial-aware Box Generation phase.

Iterations	Proportion	mAP	AP _{vt}	AP _t	AP _s	AP _m
4000	5%	35.5	17.5	42.0	37.4	26.6
20000	25%	34.2	5.3	53.4	30.9	51.8
40000	50%	34.1	7.9	50.1	34.0	52.2
80000	100%	21.0	8.0	31.4	18.8	21.9

4.3. Robustness of Point Location

To assess the robustness of our method to variations in point location, we conduct a series of detailed experiments. First, we perform the primary evaluation on the AI-TOD-v2.0 and SODA-A datasets under fully randomized point location setting ($m = 100\%$), as shown in Table 2. Compared with the results for the center-point setting in Table 1, all methods experienced some performance degradation. Point2Rbox exhibits the most significant decrease by 35.1%, as it relies on center points as priors in its label assignment strategy, which leads to substantial performance drops under randomized points. Similarly, MIL-based (*e.g.*, P2BNet, PointOBB) and CPM-based (*e.g.*, PLUG, PointOBB-v2) methods also show some decline under this condition. In contrast, our proposed denoising-based method demonstrated strong robustness, with performance decreasing by only 3.9% and 7.3% on the AI-TOD-v2.0 and SODA-A datasets, respectively. Additionally, we further analyze results for different values of the point location parameter m set to 0%, 30%, 60%, and 100%. The results, shown in Table 3, indicate that our method achieves consistently high accuracy regardless of the point location. Instead, other methods such as P2BNet and PLUG experience a more significant drop in accuracy as the point location varies. Notably, when the point is placed at the center (*i.e.*, $m = 0\%$), the accuracy is slightly lower than at $m = 30\%$ by 0.8%. This is because placing the point at the center provides prior information, leading the network to learn a central bias. In contrast, setting the point location at 30% enhances the network's robustness, resulting in more accurate predictions.

4.4. Ablation Study

This section investigates the contribution of key designs and the selection of hyper-parameters. First, we verify the effects of each module in Point Teacher. Then, we study the influence of the selection of different hyper-parameters. Note that ablations are performed on the AI-TOD-v2.0 dataset with central annotated points.

Modules in Point Teacher: To further validate the effectiveness of each module in our proposed method, we conduct ablation experiments on the AI-TOD-v2.0 dataset, with the results shown in Table 5a. When only the Spatial-aware Box Generation phase is utilized, the network initially develops spatial awareness. As a result, the accuracy remains relatively low, achieving only 21.0 AP. When the Noise-aware Label Evolution phase is introduced, the network's performance improves. The introduction of pseudo boxes by the teacher network provides supervision that improves overall performance. However, due to the coarse nature of these pseudo boxes, the accuracy increases by only 3.5%. With the addition of the DMIL module, the coarse pseudo boxes are refined, providing more stable and accurate supervision signals. Finally, with the integration of Jittering IoU Loss, the network's resistance to noisy bounding boxes is significantly enhanced, further boosting overall performance by 11.0%.

Moreover, to validate that our proposed DMIL provides more accurate supervision than MIL, we replace the DMIL with one-stage MIL and two-stage MIL* (Chen et al., 2022).

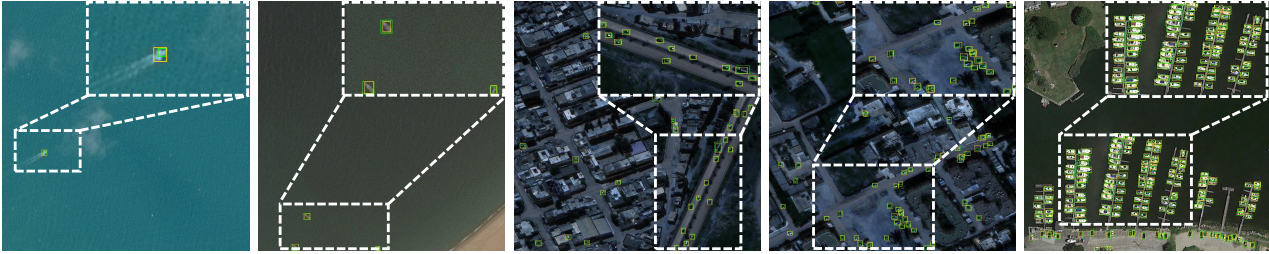


Figure 5: Visualization of pseudo boxes generated by the DMIL Module. Green boxes denote the *gt* boxes, yellow boxes denote the pseudo boxes generated by DMIL.

As shown in Table 5b, our method outperforms existing MIL approaches, achieving the highest accuracy.

$\{K_1, K_2, K_3\}$ for Pseudo Boxes Generation: K_1 , K_2 , and K_3 are hyperparameters that control the generation of pseudo boxes. Specifically, K_1 and K_2 work in tandem to guide the teacher network in producing coarse pseudo boxes, while K_3 is used in the DMIL module for Instance Selection to filter high-quality proposals. As shown in Table 5c, when K_1 and K_2 are set to 5, 3 for generating coarse pseudo boxes, the results significantly outperform those obtained with 3, 1. This is because a greater number of proposals increases the likelihood of generating more accurate boxes and aids in constructing proposals for medium-sized objects. For K_3 , a value of 1 proves more effective for small objects compared to 5, as using more proposals to refine pseudo boxes tends to result in expanded boxes, which is better suited for medium-sized objects.

r in Jittering IoU Loss: r controls the degree of perturbation in the Jittering IoU Loss. When r is set to 0, Jittering IoU Loss degrades to the standard IoU Loss. As shown in Table 5d, the best performance is achieved with r set to 0.2, while increasing r to 0.4 and 0.6 leads to a drop in accuracy. This is because a slight level of perturbation introduces a beneficial noise term in the regression process, preventing overfitting to inaccurate regression targets. However, as r increases, the perturbations become too pronounced, causing the network to learn incorrect information and resulting in a decline in accuracy.

β in DMIL Fusion: β controls the fusion weighting between coarse pseudo boxes and the proposals selected through DMIL. β is a widely used hyperparameter in generating pseudo boxes (Liu et al., 2022; Zhu et al., 2024). When β is set to 0, only the proposals filtered by DMIL are used to generate refined pseudo boxes. Conversely, when β is set to 1, only the coarse pseudo boxes are used for supervision. As shown in Table 5e, setting β to 0 can lead to object drift (*i.e.*, pseudo boxes being predicted over higher-confidence objects in dense scenarios), resulting in reduced accuracy. On the other hand, relying solely on coarse pseudo boxes with β set to 1 yields inaccurate predictions. The optimal performance is achieved by balancing the two, as combining both sources of supervision provides a more reliable outcome.

Training Time of the First Phase: The Spatial-aware Box Generation phase (*i.e.*, Phase1) occurs during the first 4000 iterations (5% of the total training iterations)

to provide the network with initial spatial awareness. To evaluate the impact of the duration of this phase on the overall network performance, we conduct experiments with varying Phase1 durations of 5%, 25%, 50%, and 100% of the total training iterations. The experimental results, as shown in Table 5f, reveal that as the proportion of Phase1 increases, network accuracy gradually declines. This behavior can be attributed to the mask-guided learning approach, which only enables the network to acquire coarse spatial awareness. This assistance does not scale with training duration, and excessively prolonged initialization reduces the time allocated for the denoising learning phase (*i.e.*, Phase2), thus deteriorating overall network performance. Notably, when Phase1 constitutes 100% of the training (with Phase2 excluded), the accuracy is significantly lower compared to when both phases are employed.

4.5. Visual Analysis

We conduct a series of analytical experiments to demonstrate that our methods can provide reliable box supervision for training. First, we visualize the pseudo boxes generated by the DMIL module and the *gt* boxes, as shown in Figure 5. The pseudo boxes generated by DMIL are more accurate and closely align with the *gt* boxes. However, in densely arranged scenes (as illustrated in the fourth column of the figure), due to DMIL's reliance on classification scores during the refinement process, instances of overlapping predictions occur. Second, we visualize the detection results of our method on the test set and compare them with the SOTA algorithm PLUG. The results are presented in Figure 6, where it can be observed that, even with only point annotations, our method can produce reasonably accurate predictions in an end-to-end training scenario.

5. Discussion

In this work, we explore the potential of detecting tiny objects with low-cost annotations, specifically leveraging point annotations. Observing the limited scale and ambiguous boundaries make it challenging to annotate accurately on the main body of the tiny object, we propose a point-robust method, Point Teacher, to address these issues.

To further advance the field of point-supervised tiny object detection, this section focuses on addressing the following three critical questions:

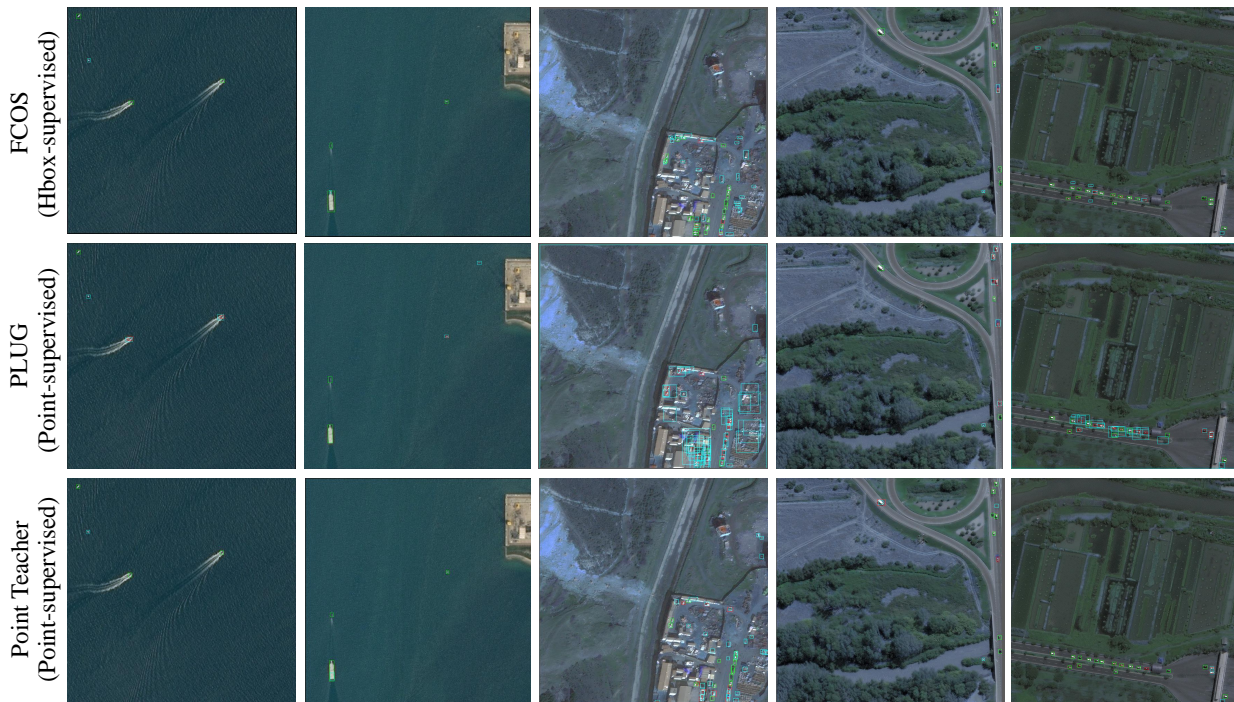


Figure 6: Visualization results on AI-TOD-v2.0 with central annotated points. The first row is the result of FCOS, the second row is the result of PLUG, and the third row is the result of Point Teacher. Green boxes denote true positive predictions, red boxes denote false negative predictions, and blue boxes denote false positive predictions.

– *Why study point supervision instead of other label-efficient methods for tiny object detection?*

Point annotations are not only well-suited to the unique characteristics of tiny objects but also strike a balance between annotation cost and detection accuracy. Due to the small scale (less than 16×16 pixels), tiny objects exhibit point-like distributions in feature maps. Compared to larger objects, point annotations provide stronger prior information, making them especially advantageous for tiny object detection. Furthermore, while point annotations are slightly more costly than image-level annotations (Chen et al., 2022), they achieve accuracy comparable to box-level annotations, offering a practical trade-off. In contrast, annotation types such as scribbles or other detailed forms introduce higher costs and often include excessive information that is redundant for tiny object detection tasks (Ren et al., 2020). Point annotations, by contrast, are precise and efficient, making them an optimal choice for annotating tiny objects.

– *Why do existing point-supervised methods perform poorly on tiny object detection?*

The weak feature representation and ambiguous boundaries of tiny objects present significant challenges for adapting existing methods to this domain. Current approaches primarily fall into three categories: MIL-based (Chen et al., 2022; Luo et al., 2024), CPM-based (He et al., 2024; Ren et al., 2024), and Auxiliary-based (Yu et al., 2024; Cao et al., 2023) methods. MIL-based methods rely on classification scores to select proposals within a bag as supervision. However, the weak features of tiny objects make it difficult to distinguish between proposals based

on classification scores, limiting the applicability of MIL-based methods to tiny object detection. CPM-based methods generate pseudo boxes using class probability map (CPM). However, the small scale and ambiguous boundaries of tiny objects undermine the boundary saliency in CPM, reducing the effectiveness of these methods. For Auxiliary-based methods (excluding SAM-based approaches), the weak feature representation of tiny objects impedes the generalization of regression training with auxiliary information, hindering further improvements in detection accuracy. In contrast, our proposed Point Teacher introduces a two-phase denoising-based paradigm, progressively refining the quality of pseudo boxes at each phase. This approach ensures more robust supervision, effectively addressing the challenges posed by tiny object detection.

– *What are the limitations of Point Teacher?*

Despite the significant advancements achieved by Point Teacher, there are remaining challenges. First, while our method excels at point-supervised tiny object detection, its performance on multi-scale objects could be further optimized. This limitation arises because the Spatial-aware Box Generation phase relies on randomly masked regions to enhance spatial awareness. However, the masks used are simple, with limited shape and color variation, which restricts the model's ability to generalize across multi-scale objects. To address this, future work could incorporate more diverse mask patterns or adopt multi-scale features in the spatial-aware phase to improve the model's generalization. Second, the challenge of accurately detecting densely packed tiny objects is further exacerbated by the position noise inherent in point

annotations, which significantly hinders precise localization. Although our method leverages spatial-aware DMIL for improved localization guidance, multiple instance learning still struggles to effectively filter pseudo boxes in densely arranged object scenarios. Future work could explore the use of vision-language models (Radford et al., 2021; Kirillov et al., 2023), which offer enhanced text-visual alignment capabilities, to provide more robust guidance in dense object arrangements.

6. Conclusion

Single point supervision offers a cost-effective solution for labeling large-scale tiny object datasets. However, the inherent challenges of tiny objects—such as their small size and weak features—make them highly sensitive to the precision of point locations. In this paper, we investigate the robustness of point-supervised tiny object detection under varying point locations and introduce Point Teacher, a robust end-to-end point-based detector. Point Teacher consists of a two-phase denoising-based learning paradigm specifically aimed at mitigating point localization noise. In the Spatial-aware Box Generation phase, spatial awareness is enhanced by randomly masked regions of the image, prompting the network to better predict spatial patterns. The Noise-aware Label Evolution phase employs a teacher-student architecture with DMIL to refine pseudo boxes and improve detection accuracy. Moreover, we introduce a novel Jittering IoU loss to prevent the model from overfitting to noisy pseudo boxes, thereby further enhancing robustness. Extensive experiments conducted on tiny object datasets demonstrate that Point Teacher surpasses existing methods, offering superior robustness and accuracy in point-supervised tiny object detection.

Acknowledgements

The research was partially supported by the National Natural Science Foundation of China (NSFC) under Grants 62271355. The numerical calculations were conducted on the supercomputing system in the Supercomputing Center, Wuhan University.

References

- Akshatha, K., Karunakar, A., Shenoy, S., Dhareshwar, C. V., Johnson, D. G. et al., 2023. Manipal-uav person detection dataset: A step towards benchmarking dataset and algorithms for small object detection. *ISPRS Journal of Photogrammetry and Remote Sensing* 195, pp. 77–89.
- Bai, Y., Zhang, Y., Ding, M. and Ghanem, B., 2018. Sod-mtgan: Small object detection via multi-task generative adversarial network. In: *European Conference on Computer Vision*, Springer, pp. 206–221.
- Cao, G., Yu, X., Yu, W., Han, X., Yang, X., Li, G., Jiao, J. and Han, Z., 2023. P2rbox: A single point is all you need for oriented object detection. *arXiv preprint arXiv:2311.13128*.
- Chen, K., Wang, J., Pang, J., Cao, Y., Xiong, Y., Li, X., Sun, S., Feng, W., Liu, Z., Xu, J., Zhang, Z., Cheng, D., Zhu, C., Cheng, T., Zhao, Q., Li, B., Lu, X., Zhu, R., Wu, Y., Dai, J., Wang, J., Shi, J., Ouyang, W., Loy, C. C. and Lin, D., 2019. MMDetection: Open mmlab detection toolbox and benchmark. *arXiv preprint arXiv:1906.07155*.
- Chen, P., Yu, X., Han, X., Hassan, N., Wang, K., Li, J., Zhao, J., Shi, H., Han, Z. and Ye, Q., 2022. Point-to-box network for accurate object detection via single point supervision. In: *European Conference on Computer Vision*, Springer, pp. 51–67.
- Chen, X., Yang, C., Mo, J., Jiang, Y. and Zheng, Z., 2024. End-to-end point supervised object detection with low-level instance features. *Applied Soft Computing* 156, pp. 111513.
- Cheng, G., Yuan, X., Yao, X., Yan, K., Zeng, Q., Xie, X. and Han, J., 2023. Towards large-scale small object detection: Survey and benchmarks. *IEEE Transactions on Pattern Analysis and Machine Intelligence* 45(11), pp. 13467–13488.
- Deng, Z., Sun, H., Zhou, S., Zhao, J., Lei, L. and Zou, H., 2018. Multi-scale object detection in remote sensing imagery with convolutional neural networks. *ISPRS Journal of Photogrammetry and Remote Sensing* 145, pp. 3–22.
- Ding, J., Xue, N., Long, Y., Xia, G.-S. and Lu, Q., 2019. Learning roi transformer for detecting oriented objects in aerial images. In: *IEEE Conference on Computer Vision and Pattern Recognition*, pp. 2849–2858.
- Gong, Y., Yu, X., Ding, Y., Peng, X., Zhao, J. and Han, Z., 2021. Effective fusion factor in fpn for tiny object detection. In: *Proceedings of the IEEE/CVF winter conference on applications of computer vision*, pp. 1160–1168.
- He, S., Zou, H., Wang, Y., Li, B., Cao, X. and Jing, N., 2024. Learning remote sensing object detection with single point supervision. *IEEE Transactions on Geoscience and Remote Sensing* 62, pp. 1–16.
- Huang, Y.-X., Liu, H.-I., Shuai, H.-H. and Cheng, W.-H., 2024. Dq-detr: Dtr with dynamic query for tiny object detection. In: *European Conference on Computer Vision*, Springer, pp. 290–305.
- Kirillov, A., Mintun, E., Ravi, N., Mao, H., Rolland, C., Gustafson, L., Xiao, T., Whitehead, S., Berg, A. C., Lo, W.-Y. et al., 2023. Segment anything. In: *Proceedings of the IEEE/CVF International Conference on Computer Vision*, pp. 4015–4026.
- Li, J., Liang, X., Wei, Y., Xu, T., Feng, J. and Yan, S., 2017. Perceptual generative adversarial networks for small object detection. In: *IEEE Conference on Computer Vision and Pattern Recognition*, pp. 1222–1230.
- Li, X., 2024. Positive-incentive noise. *IEEE Transactions on Neural Networks and Learning Systems* 35(6), pp. 8708–8714.
- Li, Y., Chen, Y., Wang, N. and Zhang, Z., 2019. Scale-aware trident networks for object detection. In: *IEEE International Conference on Computer Vision*, pp. 6054–6063.
- Lin, T.-Y., Dollar, P., Girshick, R., He, K., Hariharan, B. and Belongie, S., 2017a. Feature pyramid networks for object detection. In: *IEEE Conference on Computer Vision and Pattern Recognition*, pp. 2117–2125.
- Lin, T.-Y., Dollár, P., Girshick, R., He, K., Hariharan, B. and Belongie, S., 2017b. Feature pyramid networks for object detection. In: *Proceedings of the IEEE conference on computer vision and pattern recognition*, pp. 2117–2125.
- Lin, T.-Y., Goyal, P., Girshick, R., He, K. and Dollar, P., 2017c. Focal loss for dense object detection. In: *IEEE International Conference on Computer Vision*, pp. 2980–2988.
- Liu, C., Wang, K., Lu, H., Cao, Z. and Zhang, Z., 2022. Robust object detection with inaccurate bounding boxes. In: *European Conference on Computer Vision*, Springer, pp. 53–69.
- Liu, H.-I., Tseng, Y.-W., Chang, K.-C., Wang, P.-J., Shuai, H.-H. and Cheng, W.-H., 2024a. A denoising fpn with transformer r-cnn for tiny object detection. *IEEE Transactions on Geoscience and Remote Sensing* 62, pp. 1–15.
- Liu, J., Zhang, J., Ni, Y., Chi, W. and Qi, Z., 2024b. Small-object detection in remote sensing images with super-resolution perception. *IEEE Journal of Selected Topics in Applied Earth Observations and Remote Sensing* 17, pp. 15721–15734.
- Liu, S., Qi, L., Qin, H., Shi, J. and Jia, J., 2018. Path aggregation network for instance segmentation. In: *IEEE Conference on Computer Vision and Pattern Recognition*, pp. 8759–8768.
- Luo, J., Yang, X., Yu, Y., Li, Q., Yan, J. and Li, Y., 2024. Pointobb: Learning oriented object detection via single point supervision. In: *Proceedings of the IEEE/CVF Conference on Computer Vision and Pattern Recognition*, pp. 16730–16740.
- May, G., Dalsasso, E., Kellenberger, B. and Tuia, D., 2024. Polo – point-based, multi-class animal detection.

- Noh, J., Bae, W., Lee, W., Seo, J. and Kim, G., 2019. Better to follow, follow to be better: Towards precise supervision of feature super-resolution for small object detection. In: IEEE International Conference on Computer Vision, pp. 9725–9734.
- Oquab, M., Darcet, T., Moutakanni, T., Vo, H., Szafraniec, M., Khalidov, V., Fernandez, P., Haziza, D., Massa, F., El-Nouby, A. et al., 2023. Dinov2: Learning robust visual features without supervision. arXiv preprint arXiv:2304.07193.
- Papadopoulos, D. P., Uijlings, J. R., Keller, F. and Ferrari, V., 2017. Training object class detectors with click supervision. In: Proceedings of the IEEE Conference on Computer Vision and Pattern Recognition, pp. 6374–6383.
- Paszke, A., Gross, S., Massa, F., Lerer, A. et al., 2019. Pytorch: An imperative style, high-performance deep learning library. In: Advances in Neural Information Processing Systems, pp. 8024–8035.
- Peng, H., Xie, H., Liu, H. and Guan, X., 2024. Lgff-yolo: small object detection method of uav images based on efficient local-global feature fusion. *Journal of Real-Time Image Processing* 21(5), pp. 1–12.
- Qiao, S., Chen, L.-C. and Yuille, A., 2021. Detectors: Detecting objects with recursive feature pyramid and switchable atrous convolution. In: IEEE/CVF Conference on Computer Vision and Pattern Recognition, pp. 10208–10219.
- Radford, A., Kim, J. W., Hallacy, C., Ramesh, A., Goh, G., Agarwal, S., Sastry, G., Askell, A., Mishkin, P., Clark, J. et al., 2021. Learning transferable visual models from natural language supervision. In: International conference on machine learning, PMLR, pp. 8748–8763.
- Ren, B., Yang, X., Yu, Y., Luo, J. and Deng, Z., 2024. Pointobb-v2: Towards simpler, faster, and stronger single point supervised oriented object detection.
- Ren, S., He, K., Girshick, R. and Sun, J., 2017. Faster r-cnn: Towards real-time object detection with region proposal networks. *IEEE Transactions on Pattern Analysis and Machine Intelligence* 39(6), pp. 1137–1149.
- Ren, Z., Yu, Z., Yang, X., Liu, M.-Y., Schwing, A. G. and Kautz, J., 2020. Ufo 2: A unified framework towards omni-supervised object detection. In: European conference on computer vision, Springer, pp. 288–313.
- Russakovsky, O., Deng, J., Su, H., Krause, J., Satheesh, S., Ma, S., Huang, Z., Karpathy, A., Khosla, A., Bernstein, M. et al., 2015. Imagenet large scale visual recognition challenge. *International Journal of Computer Vision* 115(3), pp. 211–252.
- Shi, S., Fang, Q., Zhao, T. and Xu, X., 2024. Similarity distance-based label assignment for tiny object detection. arXiv preprint arXiv:2407.02394.
- Singh, B. and Davis, L. S., 2018. An analysis of scale invariance in object detection snip. In: IEEE Conference on Computer Vision and Pattern Recognition, pp. 3578–3587.
- Singh, B., Najibi, M. and Davis, L. S., 2018. Sniper: Efficient multi-scale training. In: Advances in Neural Information Processing Systems, pp. 9310–9320.
- Tan, M., Pang, R. and Le, Q. V., 2020. Efficientdet: Scalable and efficient object detection. In: IEEE Conference on Computer Vision and Pattern Recognition, pp. 10781–10790.
- Tang, J., Cheng, J., Xiang, D. and Hu, C., 2022. Large-difference-scale target detection using a revised bhattacharyya distance in sar images. *IEEE Geoscience and Remote Sensing Letters* 19, pp. 1–5.
- Tian, Z., Shen, C., Chen, H. and He, T., 2019. Fcos: Fully convolutional one-stage object detection. In: Proceedings of the IEEE/CVF international conference on computer vision, pp. 9627–9636.
- Wang, J., Yang, W., Guo, H., Zhang, R. and Xia, G.-S., 2021. Tiny object detection in aerial images. In: International Conference on Pattern Recognition, pp. 3791–3798.
- Wang, L., Zhou, Z., Shi, G., Guo, J. and Liu, Z., 2024. Small object detection based on bidirectional feature fusion and multi-scale distillation. In: International Conference on Artificial Neural Networks, Springer, pp. 200–214.
- Wang, P., Cai, Z., Yang, H., Swaminathan, G., Vasconcelos, N., Schiele, B. and Soatto, S., 2022. Omni-detr: Omni-supervised object detection with transformers. In: Proceedings of the IEEE/CVF conference on computer vision and pattern recognition, pp. 9367–9376.
- Wu, D., Chen, P., Yu, X., Li, G., Han, Z. and Jiao, J., 2023. Spatial self-distillation for object detection with inaccurate bounding boxes. In: Proceedings of the IEEE/CVF International Conference on Computer Vision, pp. 6855–6865.
- Xiao, Y., Xu, T., Yu, X., Fang, Y. and Li, J., 2024. A lightweight fusion strategy with enhanced interlayer feature correlation for small object detection. *IEEE Transactions on Geoscience and Remote Sensing* 62, pp. 1–11.
- Xie, X., Cheng, G., Wang, J., Yao, X. and Han, J., 2021. Oriented r-cnn for object detection. In: Proceedings of the IEEE/CVF international conference on computer vision, pp. 3520–3529.
- Xu, C., Ding, J., Wang, J., Yang, W., Yu, H., Yu, L. and Xia, G.-S., 2023. Dynamic coarse-to-fine learning for oriented tiny object detection. In: IEEE Conference on Computer Vision and Pattern Recognition, pp. 7318–7328.
- Xu, C., Wang, J., Yang, W. and Yu, L., 2021a. Dot distance for tiny object detection in aerial images. In: IEEE Conference on Computer Vision and Pattern Recognition Workshops, pp. 1192–1201.
- Xu, C., Wang, J., Yang, W., Yu, H., Yu, L. and Xia, G.-S., 2022a. Detecting tiny objects in aerial images: A normalized wasserstein distance and a new benchmark. In: ISPRS Journal of Photogrammetry and Remote Sensing, Vol. 190, pp. 79–93.
- Xu, C., Wang, J., Yang, W., Yu, H., Yu, L. and Xia, G.-S., 2022b. Rfla: Gaussian receptive field based label assignment for tiny object detection. In: European conference on computer vision, Springer, pp. 526–543.
- Xu, M., Zhang, Z., Hu, H., Wang, J., Wang, L., Wei, F., Bai, X. and Liu, Z., 2021b. End-to-end semi-supervised object detection with soft teacher. In: Proceedings of the IEEE/CVF international conference on computer vision, pp. 3060–3069.
- Yu, X., Gong, Y., Jiang, N., Ye, Q. and Han, Z., 2020. Scale match for tiny person detection. In: IEEE Workshops on Applications of Computer Vision, pp. 1257–1265.
- Yu, Y., Yang, X., Li, Q., Da, F., Dai, J., Qiao, Y. and Yan, J., 2024. Point2rbox: Combine knowledge from synthetic visual patterns for end-to-end oriented object detection with single point supervision. In: Proceedings of the IEEE/CVF Conference on Computer Vision and Pattern Recognition, pp. 16783–16793.
- Zhang, S., Long, J., Xu, Y. and Mei, S., 2024. Pmho: Point-supervised oriented object detection based on segmentation-driven proposal generation. *IEEE Transactions on Geoscience and Remote Sensing* 62, pp. 1–18.
- Zhang, S., Wang, Z. and Ke, W., 2025. One point is all you need for weakly supervised object detection. *Pattern Recognition* 159, pp. 111087.
- Zhao, Z., Du, J., Li, C., Fang, X., Xiao, Y. and Tang, J., 2024. Dense tiny object detection: A scene context guided approach and a unified benchmark. *IEEE Transactions on Geoscience and Remote Sensing* 62, pp. 1–13.
- Zheng, Z., Zhong, Y., Ma, A., Han, X., Zhao, J., Liu, Y. and Zhang, L., 2020. Hynet: Hyper-scale object detection network framework for multiple spatial resolution remote sensing imagery. *ISPRS Journal of Photogrammetry and Remote Sensing* 166, pp. 1–14.
- Zhou, Y., Yang, X., Zhang, G., Wang, J., Liu, Y., Hou, L., Jiang, X., Liu, X., Yan, J., Lyu, C. et al., 2022. Mmrotate: A rotated object detection benchmark using pytorch. In: Proceedings of the 30th ACM International Conference on Multimedia, pp. 7331–7334.
- Zhu, H., Xu, C., Yang, W., Zhang, R., Zhang, Y. and Xia, G.-S., 2024. Robust tiny object detection in aerial images amidst label noise. arXiv preprint arXiv:2401.08056.